THE JOURNAL OF PHYSICAL CHEMISTRY C
A JOURNAL OF THE AMERICAN CHEMICAL SOCIETY

pubs.acs.org/JPCC

Article

A Step in Carbon Capture from Wet Gases: Understanding the Effect of Water on CO_2 Adsorption and Diffusion in UiO-66

Yann Magnin,* Estelle Dirand, Alejandro Orsikowsky, Mélanie Plainchault, Véronique Pugnet, Philippe Cordier, and Philip L. Llewellyn

Cite This: https://doi.org/10.1021/acs.jpcc.1c09914

Read Online

ACCESS | Metrics & More | Article Recommendations | Supporting Information

ABSTRACT: Understanding the role played by moisture in CO_2 sorption is key for designing the next generation of solid sorbents such as metal−organic frameworks, which can be used for carbon capture and conversion as well as for molecular sieving, energy storage, *etc.* The abundance of water in nature and industrial processes, including in anthropogenic sources of CO_2 has been shown to significantly affect commercial adsorbent performances, including their uptake capacity and selectivity. However, less is known about the role of humidity on CO_2 diffusion, even though it is crucial for economically viable rapid capture processes. In this work, we have used atomistic simulations and experiments to gain insight into the effect of humidity on CO_2 adsorption, diffusion and transport properties in UiO-66(Zr), here described as a flexible structure. We show that depending on the water concentration adsorbed in the host nanoporosity, the CO_2 adsorption can be enhanced or reduced depending on thermodynamic conditions. At low water loading, isolated molecules interact with low-energy sites of the sorbent. At higher loading, nucleation drives water cluster formation, followed by cluster percolation resulting in a sub-nanoporous adsorbing media decreasing the overall CO_2 diffusion compared to the dry structures. We finally show that equilibrium parameters such as self-diffusion coefficients and isotherms can be used to describe the CO_2 transport in dry and humid structures through the nano-Darcy equation.

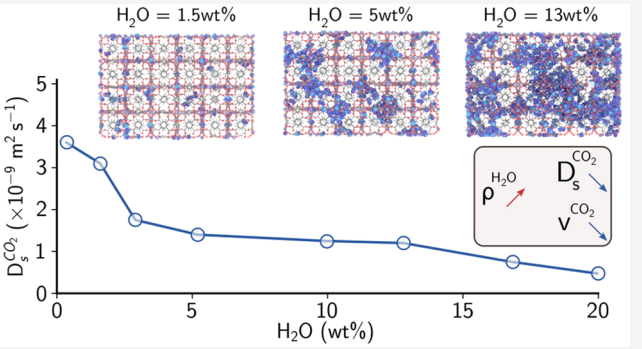

INTRODUCTION

The management and abatement of greenhouse gases, with their effect on climate change can be considered as one of the great worldwide challenges of our century. Along with better energy efficiency and the replacement of fossil fuels by renewable energy, carbon capture and storage (CCS) is an important tool to meet this challenge.[1,2] Furthermore, if the geologically stored carbon is captured from the atmosphere (direct air capture, DACCS) or from bioenergy conversion (BECCS), then both DACCS and BECCS, as negative emission technologies, are important means to remove historical emissions.[3,4] The first brick in the CCS chain is capture, which is often considered the most expensive block.[5] This explains why significant research and development is devoted to finding economic alternatives to the canonical amine scrubbing approach, where the thermal regeneration step tends to be highly energy consuming. Adsorption-based methods can be considered of interest, although they equally suffer from their own disadvantages such as insufficient CO_2 product purity.[6,7] Nevertheless, CO_2 adsorption in porous solids has drawn widespread attention due to their low regeneration energy requirements.[8] Materials such as porous carbon,[9] clay,[10] silica,[11] zeolites,[12] covalent organic polymers,[13] covalent organic frameworks,[14] and metal organic frameworks (MOFs)[15] have been shown to have the ability to capture CO_2 molecules from anthropogenic sources or directly from the air. Of these adsorbents, MOFs are nano- and/or mesoporous synthetic materials, composed of metal ion/oxide nodes coordinated by organic ligands. Their frameworks are comparable to molecular "interlocking building bricks" (such as Lego), having a quasi-infinite tunability with respect to their pore sizes and reactivity depending on their metal, ligand type, and overall chemistry.[16] Such a unique versatility makes MOFs potentially key materials for applications such as molecular capture, conversion, sieving, energy storage, and even drug delivery.[17]

One focus of adsorption-based CO_2 capture research concerns the effect of water on CO_2 capacity and selectivity. While one can dry the flue gas stream, this comes at an

Received: November 19, 2021
Revised: January 13, 2022

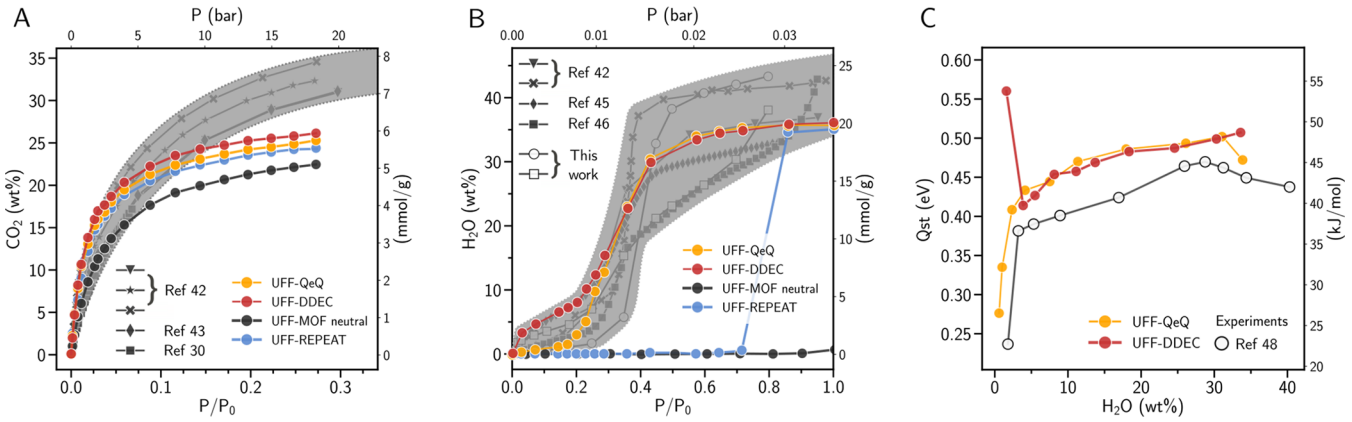

Figure 1. (A) CO_2 isotherms at T = 300 K in UiO-66. The black circles correspond to a neutral MOF, where Coulomb interactions have been turned off. The red, blue, and yellow plots correspond to isotherms calculated using DDEC, REPEAT, and QeQ point charges, respectively. The gray area delimits different experimental isotherms at T = 300 K from volumetry experiments. (B) H_2O isotherms at T = 300 K in UiO-66; colored circle plots correspond to the same point charges in part A. (C) Water isosteric heat of adsorption as a function of the water loading. The red and yellow plots correspond to DDEC and QeQ point charges, respectively. The white circles correspond to experiments.

expense,[18,19] so approaches which allow some degree of humidity in the separation are of interest. Adsorption properties have been extensively studied in a large number of MOFs and in hypothetical structures emerging from machine learning, but surprisingly, little is known about the role of water on CO_2 diffusion, nevertheless present in the different stream sources. Indeed, solid porous adsorbents, usually optimized for CO_2/N_2 separations, have been reported to be poorly efficient in real-life applications where humid steams are present.[20] In such situations, water most often acts as a CO_2 competitor, resulting in a loss of adsorbent selectivity. On the other hand, at the laboratory scale, limited amounts of humidity have even been shown to increase the CO_2 adsorption properties of adsorbents.[21−24]

A second focus for CO_2 capture research relates to intensification, and one example concerns the development of rapid processes. Indeed, adsorption-based processes can be accelerated with minute-long cycles possible in both rapid-PSA (pressure swing adsorption) and rapid-TSA (temperature swing adsorption).[6,7] In such cycles, while equilibrium thermodynamics can give some insight, there is a need to understand the diffusion behavior of the CO_2 and, in the present case, the pore diffusion of CO_2 in the presence of humidity. Hence, in this work, we investigate the interplay of thermodynamics in both CO_2 and H_2O diffusion and transport for a wide range of water loadings confined into the UiO-66(Zr) porosity.

METHODS

Adsorption isotherms and diffusion coefficients of guest molecules were determined by Monte Carlo simulations[25] in the osmotic ensemble.[26] To account for ideal gas deviation, pressures (P) have been corrected by the Soave−Redlich−Kwong model.[27] Diffusion has been studied by molecular dynamics simulations in the isothermal−isobaric ensemble.[25] For both algorithms, we have used the massively parallel LAMMPS code.[28] Simulation details are provided in the Supporting Information.

The MOF structure used in simulations consists of 3 × 2 × 2 UiO-66 supercells of about 6 × 4 × 4 nm^3 (Figure S1 in the Supporting Information). A dehydroxylated UiO-66 structure has been chosen to compare simulations and experiments, where thermal pretreatments are generally applied prior to adsorption. Such treatments are made to remove adsorbates and *N*,*N*-dimethylformamide, known to affect the structure by removing a fraction of H atoms from hydroxyl groups.[29,30] MOF bonds were modeled by the universal force field (UFF),[31] previously demonstrated to well reproduce the poromechanical properties of the pristine and adsorbate-free structure.[32] While UiO-66 is considered as a rigid structure with a Young's modulus ∼40 GPa,[32] flexibility has mainly accounted for its effect on molecular diffusion.[33] However, it is worth noting that, at equilibrium, a slight contraction of the sorbent by ∼1% has been found depending on the adsorbate type and loading (Figure S2). In order to validate the choice of the UFF force field, our results have been compared to experiments (parameters are given in ref 34 and in Tables S1 and S2 in the Supporting Information). The MOF point charges were taken from the literature, chosen in order to cover different determination techniques such as DFT with REPEAT[35] and DDEC[36] models, and from the empirical QeQ technique.[37] Intermolecular interactions were ensured by the long-range CO_2 Trappe potential (with a cutoff of 1 nm)[38] and by the four points long-range TIP4P-Ew[39] for H_2O (with a cutoff of 0.85 nm). In addition, a long-range Coulombic solver (Ewald summation) was applied for all interactions, for MOF atoms as well as for CO_2 and H_2O molecules. Guest−host interactions have been modeled from the Lennard-Jones potential, while the Lorentz−Berthelot mixing rule was used for crossed interatomic terms. Simulation and experimental details and methods applied to perform continuous water cluster representations and cluster size analyzes are detailed in the Supporting Information.

RESULTS AND DISCUSSION

Single Component Adsorption Isotherms. The CO_2 adsorption isotherms have been calculated at T = 300 K, with different point charges and a neutral structure (Coulomb interactions turned off), and compared to experimental isotherms of fully outgassed UiO-66. CO_2 isotherms are Langmuirian, characteristic of nanoporous adsorbing materials, with preferential uptake at low P and showing continuous uptake with increasing P. One observes a favored adsorption in the tetrahedral cages below a relative CO_2 pressure P/P_0 of

https://doi.org/10.1021/acs.jpcc.1c09914
J. Phys. Chem. C XXXX, XXX, XXX−XXX

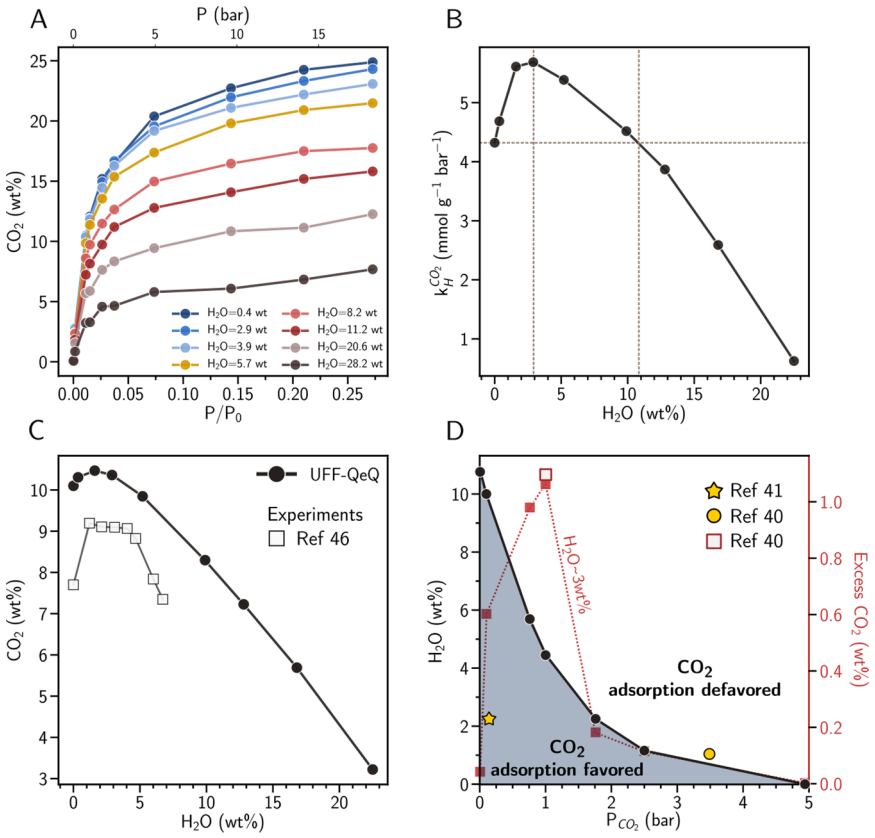

Figure 2. (A) CO_2 isotherms for different preadsorbed water loadings into UiO-66 at T = 300 K. (B) CO_2 Henry's constants as a function of the water loading at T = 300 K. (C) Evolution of the CO_2 uptake as a function of water loading at P_{CO_2} = 1 bar and T = 300 K. The black circles correspond to simulations; the white squares correspond to TGA experiments. (D) Multicomponent adsorption diagram representing water uptake as a function of the CO_2 pressure determined from simulations. Parameters showing an excess in CO_2 uptake correspond to the gray area. CO_2 excess is shown for a water loading of 3 wt % by the red dashed squares plot. Results are compared with works of the literature: yellow star, yellow circle, and white square.

~0.03 (attributed to the size entropy effect[40]) and in larger octahedral cages above it.[41] Experimental data are presented in the gray area (Figure 1A), highlighting dispersion in results from various samples and groups,[30,42,43] and can be explained by various synthesis approaches that can lead to samples with varying amount of defects.[41] On the other hand, computationally, while Coulomb interactions are found to increase the CO_2 adsorption by a few wt % (colored circle versus black circle plots), small differences are found depending on the MOF point charges employed. It is noteworthy that, when comparing simulations to experiments, Henry constants are slightly overestimated, while CO_2 uptakes are underestimated for a pressure above a P/P_0 of ~0.075. Such discrepancies, also found in other works,[40,42,44] may be due to the CO_2 Trappe potential[38] at low loading and to the lack of defects and intergrain batch porosity for larger CO_2 loading. H_2O adsorption isotherms have been calculated at T = 300 K, with the same MOF point charges as for CO_2 sorption, and then compared to experiments[42,45,46] (Figure 1B). Depending on the pressure range, isotherms show both hydrophobic and hydrophilic behaviors, respectively, below and above a relative pressure P/P_0 of about ~0.25. Contrary to CO_2, the MOF point charges lead to strong discrepancies in H_2O isotherms. While isotherms based on DDEC[36] and QeQ[37] agree with experiments, REPEAT[35] presents a strong shift in relative pressure of CO_2 uptake, predicting a spurious hydrophobic host. In the hydrophobic pressure range (P/P_0 < 0.25), we also notice differences between DDEC, showing a finite sorption behavior in good agreement with the isotherm proposed by Canivet et al.,[45] and QeQ, showing a more hydrophobic behavior in good agreement with the experiments of Chanut et al.[46] The shape presented by DDEC (red circles) has been attributed to the presence of defects in MOF structures,[41,47] promoting the formation of water bridges between defective sites at low P, making the host more hydrophilic. With the structure used in these simulations (free of defects), we then plot the isosteric heat of adsorption (Figure1C). The two models compare well to experimental values found in the literature,[48] except for water loading below a few percent, where DDEC predicts a slight hydrophilic behavior, in line with the corresponding isotherm shape (red circles in Figure1B). One can take this analysis one step further and compare the per-water average energy. At T = 5 K, the two models show a decreasing energy as a function of the loading (Figure S3A), with a lower energy for DDEC, explained by larger charges on metal/oxide nodes compared to QeQ. However, when comparing the per-water energy at T = 300 K, plots show an antagonist behavior (Figure S3B), where the DDEC model presents an increasing energy, while QeQ decreases (also visible in the isosteric heat of adsorption in Figure1C). In addition, we also note that, depending on the charge model used, water adsorption is found to be favored in UiO-66 tetrahedral cages with DDEC, in agreement with the DFT calculations of Glover et al.,[41] while it is favored in

https://doi.org/10.1021/acs.jpcc.1c09914
J. Phys. Chem. C XXXX, XXX, XXX−XXX

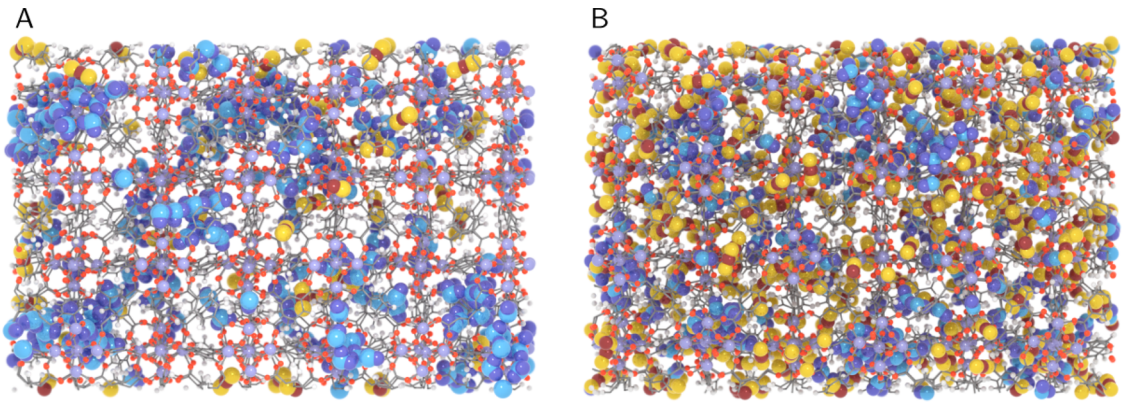

Figure 3. (A) MOF with multicomponent guests adsorbed at a water loading of about 5 wt % and a CO_2 pressure of 0.1 bar. Water molecules correspond to the light and dark blue atoms; CO_2 molecules correspond to the brown and yellow atoms. (B) Same as part A at a CO_2 pressure of 2 bar.

octahedral cages with QeQ, in agreement with the work proposed by Calero et al.[40] (Figure S4A−D). Based on these results, we chose the QeQ point charges for the following calculations, setting aside the DDEC model that we find less adapted to describe thermodynamic behaviors of the system.

It is important to note that no universally accepted point charge model exists for now and that charges are not experimentally observable, making direct comparisons with experiments almost impossible. In the past decades, several methods have been developed to determine point charges, mostly *ab initio* and DFT methods, followed by theoretical analyses targeting the best point charges able to fit the full electronic configuration of a system. However, the determination of charges suffers from a lack of clarity since it has been shown that values depend on the quantum numerical technique used, basis set size, theoretical charge determination approach and that it is impossible to exactly reproduce the continuous nature of the electron density distribution of a system.[49] For these reasons, the available charge sets present widely dispersed numerical values[50] and need to be carefully selected and further confirmed by experiments.

Multicomponent Adsorption Isotherms. In order to characterize the role played by water molecules on CO_2 adsorption, we used equilibrated structures of Figure 1B as initial humid hosts for a series of CO_2 adsorptions. In Figure 2A, we show the CO_2 isotherms for water loadings ranging from 0 to ∼28 wt %. For a relative CO_2 pressure P/P_0 of > 0.013, an increase of the water content tends to decrease the CO_2 uptake due to the pore volume occupation. However, at very low P/P_0, Henry's constant (*i.e.*, the slope of isotherms in the low pressure range) shows a nonmonotonic shape, indicating that the water acts (in addition to the MOF) as a supplemental driving force favoring the CO_2 sorption. Hence, at low P/P_0, water is shown to dope CO_2 affinity up to ∼11 wt %, with a maximum found at 3 wt % water (dashed lines in Figure 2B). From isotherms presented in Figure 2A, we then plot the CO_2 uptake as a function of the water loading at P_{CO_2} = 1 bar and T = 300 K (Figure 2C). In the latter, simulations are compared to thermogravimetric analysis experiments (TGA) under similar thermodynamic conditions.[46] Both approaches mirror the initial increase in CO_2 uptake at low water loading, followed by a decrease for larger loadings. With the experiments being limited to P_{CO_2} = 1 bar, we have extended it for other CO_2 pressures. By measuring the range of water where an excess of CO_2 is observed compared to the dry MOF for several P_{CO_2} values from simulations (Figure S5), we propose a multicomponent adsorption diagram in Figure 2D. The gray area shows conditions where preadsorbed water molecules induce an excess in CO_2 uptake (compared to dry MOF) and where red squares quantify the CO_2 excess as a function of P_{CO_2} at 3 wt % water. Hence, we observe a maximum of excess CO_2 of about 1 wt % at P_{CO_2} = 1 bar. These results suggest that water tends to promote CO_2 adsorption, further compatible to anthropogenic capture applications with CO_2 partial pressures ranging from 0.1 to 0.2 bar. It is worth noting that DFT calculations have also demonstrated the beneficial role of preadsorbed water in some MOFs, increasing the CO_2/N_2 selectivity due to the larger interaction energy between CO_2 and H_2O, in combination with a higher CO_2 uptake.[24] Such results, comparable to the calculations of Calero et al.[40] (white square and yellow circle in Figure 2D), have been attributed to extra adsorption at water occupying octahedral cages of the UiO-66. Indeed, such cages are not favored locations for CO_2 in the dry structure when P_{CO_2} < 1 bar, while the presence of water proffers additional CO_2 capture sites. The electric field created by the adsorbed water acts as a driving force attracting the CO_2 quadrupole moment promoting adsorption. Such a behavior is consistent with this work, where water bridges are found in octahedral cages (Figure S4A,C) with depleted tetrahedral cavities at around 3 wt % water, corresponding to the maximum in $k_H^{CO_2}$ and CO_2 uptake (Figure 2B,C). This can also be seen in Figure 3A, where CO_2 molecules are mainly found to be adsorbed near water in octahedral cages at low P_{CO_2} and then in tetrahedral ones at larger P_{CO_2} (Figure 3B). For larger water loadings, clusters start forming in tetrahedral cages (Figure S4D), competing with CO_2 and driving a decrease in both $k_H^{CO_2}$ and CO_2 uptake. It is interesting to note that such selectivity in adsorption sites is coherent with observations made elsewhere,[40] showing that CO_2−H_2O interactions are favored when P_{CO_2} < 1 bar, while CO_2−CO_2 interactions are favored above it and should correspond to conditions where CO_2 starts adsorbing in octahedral cages. We can extend this analysis to defective structures shown to favor water adsorption, making the MOF structure more hydrophilic.[47] In the case of missing linkers in a UiO-66, water bridges have been evidenced to play the role of "pseudolinkers" by connecting unlinked metal/

https://doi.org/10.1021/acs.jpcc.1c09914
J. Phys. Chem. C XXXX, XXX, XXX−XXX

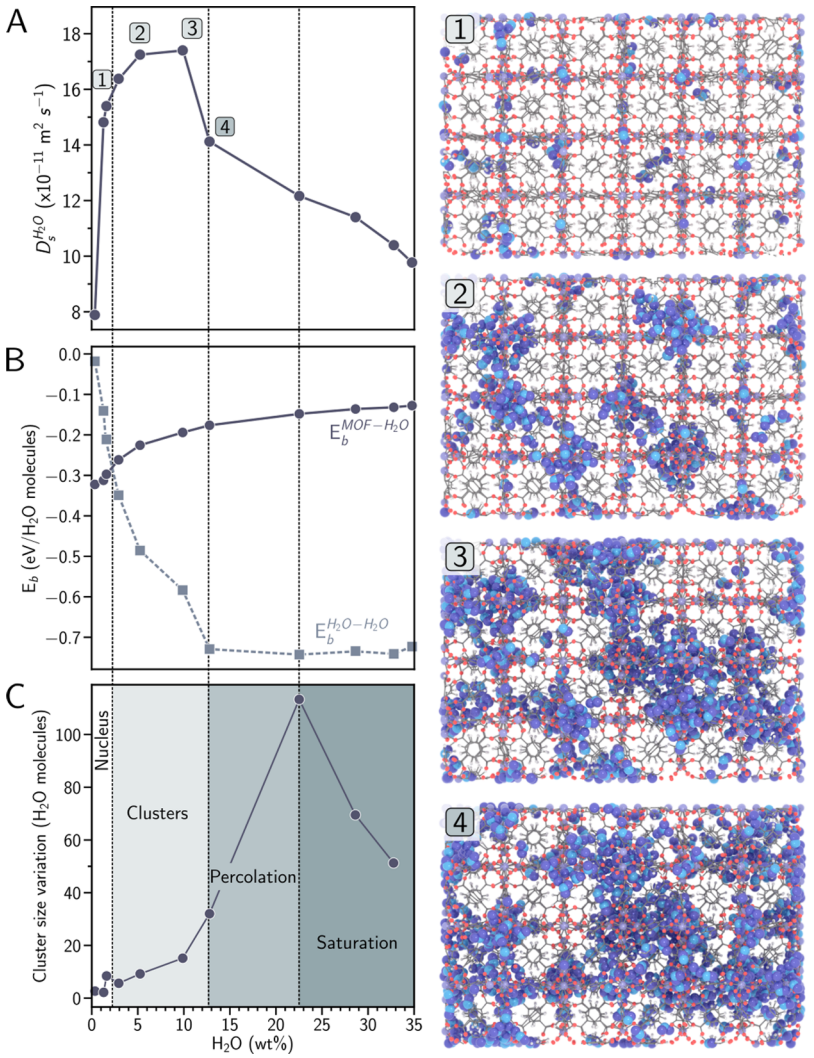

Figure 4. (A) Self-diffusion coefficient of H_2O as of function of the water loading. Indexes correspond to the snapshots shown in the right panel, representing water at 1 wt % (1), 5 wt % (2), 10 wt % (3), and 13 wt % (4). (B) MOF−water binding energy (dark gray circles, solid line) and water−water binding energy (free of MOF structure) as a function of the water loading (light gray circles, dashed line). (C) Cluster size variation in the MOF structure as a function the water loading. The different background colors correspond to isolated water adsorbates on metal/oxide nodes (white), water clusters (light gray), cluster percolation (medium gray), and saturation (dark gray).

oxide nodes.[51] Resulting structures thus present smaller pores with an increase in attractive porous surfaces favoring CO_2 adsorption. Such a behavior tends to lower the range of P_{CO_2} where an excess in CO_2 adsorption can occur, as shown by the yellow star[41] in Figure 2D.

Single Component H_2O Diffusion. The self-diffusion coefficient (D_s) is investigated by molecular dynamic simulations, using the mean square displacement approach

$$\lim_{t\to\infty} \frac{1}{N} \sum_{i=1}^{N} |r_i(t) - r_i(t_0)|^2 = 2dD_s t^{\alpha} \quad (1)$$

where D_s is shown to scale as a function of the square displacement of molecules, spanning an infinite time period (Figure S6). In eq 1, r is the position of a molecule i at time t, and the normalized summation over N molecules corresponds to the ensemble average at thermodynamic equilibrium. The parameter d corresponds to the dimension of the system, and α is an exponent referring to diffusion modes: pseudo-Fickian <1, Fickian ∼1, and anomalous >1.[52] Pseudo-Fickian diffusion behavior usually occurs in high-confinement environments, where molecules are in a diffusive regime, jumping from a low-energy site to another.[53,54] In such situations, the diffusion is mainly driven by the guest−host interactions, largely differing from the bulk phase.[55,56]

The nonmonotonic D_s behavior in Figure 4A is insight from binding energies and cluster analysis. Guest−host binding is defined as $E_b^{MOF-H_2O} = E_{MOF+H_2O} - E_{MOF} - E_{H_2O}$, with E_{MOF+H_2O} the potential energy of the MOF including adsorbed water molecules, E_{MOF} the MOF energy after removing water, and E_{H_2O} the energy of water molecules after removing the MOF structure. We also define interwater binding, corresponding to the energy variation of the water volume when removing one molecule from it, $E_b^{H_2O-H_2O} = E_{H_2O} - E_{H_2O-1}$. At very low loading (<1.5 wt %), isolated water molecules are strongly bound to metal/oxide nodes, showing a large adsorbate−adsorbent binding energy $E_b^{MOF-H_2O}$ (solid line), compared to the adsorbate−adsorbate $E_b^{H_2O-H_2O}$ of ∼0 (dashed line; Figure 4B). This is further confirmed by the cluster size evolution (found to be at 1 molecule in Figure S7),

https://doi.org/10.1021/acs.jpcc.1c09914
J. Phys. Chem. C XXXX, XXX, XXX−XXX

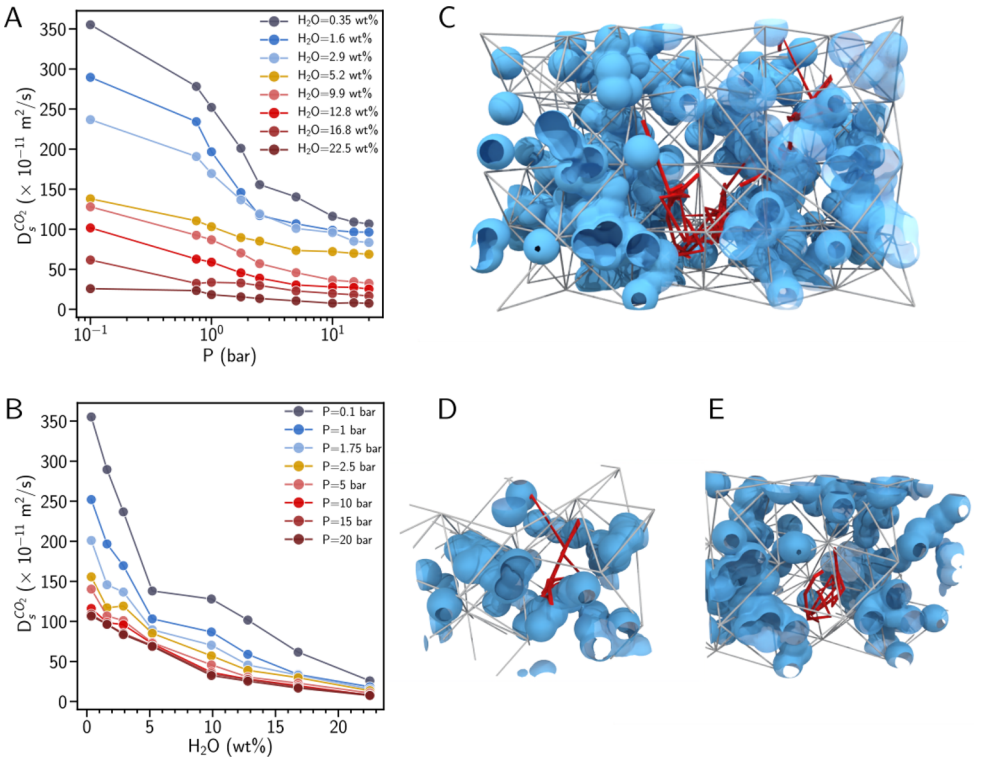

Figure 5. (A) Self-diffusion coefficient of CO_2 as of function of pressure for different water loadings (colored circle plots). (B) Self-diffusion coefficient of CO_2 as of function of the water loading for different CO_2 pressures (colored circle plots). (C) Snapshot of a CO_2 trajectory in wet UiO-66. This simplified view shows the MOF structure (light gray sticks) filled by continuous water cluster volumes (blue surfaces) and the CO_2 trajectory (red line). (D) Trajectory of a CO_2 molecule (red line) jumping from one water cluster surface to another (blue surfaces). (E) Trajectory of a CO_2 molecule (red line) trapped in a tetrahedral cage of MOF surrounded by water clusters (blue surfaces).

and by the lack of cluster size variation in Figure 4C. For larger loadings (but still <3 wt %), isolated water molecules nucleate to form chains, bridging adjacent metal/oxide nodes in octahedral MOF cages (Figure S4A,C) and corresponding to the small jump in Figure 4C. In this region, water presents a moderate diffusivity. At around 3 wt %, $E_b^{MOF-H_2O} = E_b^{H_2O-H_2O}$, water clusters start forming in tetrahedral cages (Figure 4C and Figure S4D), and $E_b^{MOF-H_2O}$ increases (binding decreases), while $E_b^{H_2O-H_2O}$ decreases (more stable water clusters). Clusters forming in tetrahedral cages present weaker interactions with the MOF structure (larger $E_b^{MOF-H_2O}$), favoring clusters hopping in neighboring cages, increasing D_s with a maximum found between ∼5 and ∼10 wt %. This loading corresponds to a change from the hydrophobic to the hydrophilic region in the isotherm (Figure 1B). In other words, when water clusters form, the dynamic properties of the guest molecules change, here counterintuitively increasing water diffusion with a larger number of guests water. This increase is supported by the fact that the type-V H_2O isotherm is characteristic of weak adsorbate−adsorbent interactions. In the present case, when H bonds of water molecules become larger than the ones lying at the adsorbate−adsorbent interface, $E_b^{MOF-H_2O} > E_b^{H_2O-H_2O}$, the diffusion increases. Above ∼13 wt %, clusters grow (Figure 4C), and the water network percolates, limiting the diffusion of the overall water network. Above ∼22 wt %, cluster size variation decreases (Figure 4C), indicating that the MOF-free volume is almost fully occupied. Such results are consistent with experiments conducted by Hossain and Glover,[57] where water transport diffusivity was determined from the concentration swing frequency response (CSFR) in UiO-66 particles. DFT simulations conducted to support experiments have revealed that water molecules selectively adsorbed in one type of cage at low loading tend to spread to other cages at larger loading, connecting both tetrahedral and octahedral cavities (water cluster coalescence), corresponding to the percolation phenomenon discussed above. Interestingly, a minimum in transport diffusivity has been reported at 7.2 wt %. Transport diffusivity (differing from self-diffusivity) typically increases with loading due to an increasing thermodynamic factor.[56,58,59] When clusters form, the transport diffusivity is slowed because the increase in hydrogen bonding to clusters decreases the transport rate until pore lining/filling occurs. The minimum in transport diffusivity thus corresponds to the maximum of the self-diffusivity found between ∼5 and ∼10 wt %, in agreement with the experimental results discussed above.

Multicomponent CO_2 Diffusion. It is possible to provide some insight regarding the role played by moisture on the equilibrium diffusion parameters of the CO_2. As previously shown for pure water, $D_s^{CO_2}$ is determined for different water loadings preadsorbed in the UiO-66 structure (Figure S6). In Figure 5A, we show the self-diffusion coefficient of CO_2 at T = 300 K as a function of P_{CO_2} for different water loadings.

In an almost dry MOF (gray circles) with $P_{CO_2} < 1$ bar, CO_2 adsorption mainly occurs in tetrahedral cages and CO_2 diffusing by hopping trough octahedral cavities. Above that pressure, molecules start adsorbing in octahedral cages, and the concomitant free pore volume decrease drives a drop in $D_s^{CO_2}$. At a P_{CO_2} of ∼2 bar, MOF cavities are largely filled by molecules (Figure 3B). The increase of guest−guest collisions thus shows a slight drop in $D_s^{CO_2}$ when $P_{CO_2} > 2$ bar. This behavior is reminiscent of that when increasing the water

https://doi.org/10.1021/acs.jpcc.1c09914
J. Phys. Chem. C XXXX, XXX, XXX−XXX

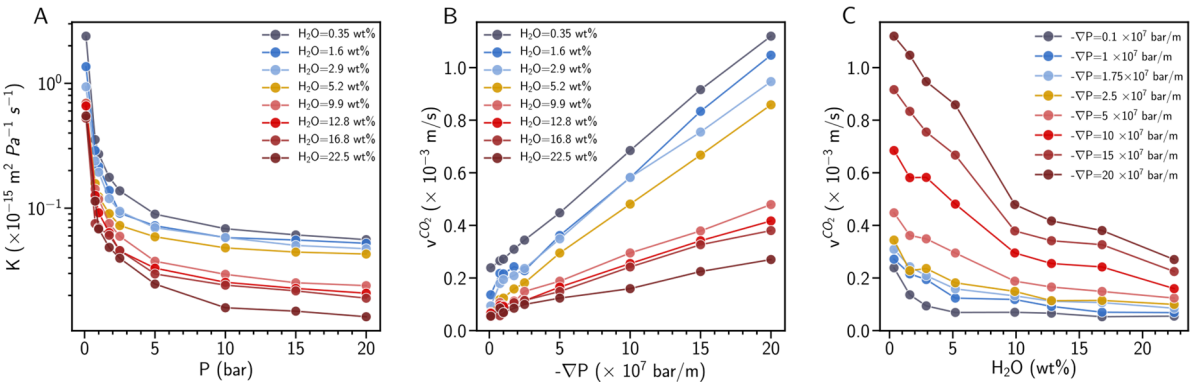

Figure 6. (A) Water permeance of the UiO-66 structure as a function of the CO_2 pressure for different water concentrations (colored circles plots). (B) Nano-Darcy flow velocity as a function of the pressure gradient for different water concentrations (colored circles plots). The pressure gradient is based on driving pressure ranging from 0 to 20 bar. (C) Nano-Darcy's flow velocity as a function of the water loading for different CO_2 pressure gradients (colored circles plots). The pressure gradient is based on driving pressure ranging from 0 to 20 bar applied in a MOF of 100 nm length in the flowing direction.

loading up to 3 wt % (light blue circles). Remember that this water threshold corresponds to a situation where water molecules preferentially adsorbed octahedral cages, leaving CO_2 molecules free to diffuse through tetrahedral ones. For the overall water loadings, $D_s^{CO_2}$ is found to decrease when the water loading increases. Such a behavior can be intuitively understood from previous thermodynamic results, suggesting that the water acts as an extra sorbing media, limiting the CO_2 diffusion (Figure 5B). This is illustrated in Figure 5C, where a CO_2 trajectory is sketched inside a wet UiO-66, proposed in a simplified representation. In it, the MOF is presented as light gray sticks crossing at the center of mass of metal/oxide nodes. The water clusters are modeled by transforming the set of discrete water molecules into continuous surfaces (blue volume). The CO_2 trajectory (red line) shows hopping in the free volume of the wet MOF structure. The CO_2 trajectory thus shows hopping from attractive surfaces of water clusters through depleted cages (Figure 5D) or being trapped in a depleted cage surrounded by water clusters (Figure 5E). It is interesting to notice that when $P_{CO_2} < 1$ bar, CO_2–H_2O is favored compared to CO_2–CO_2 interactions,[40] in agreement with observations made in Figure 5. Such CO_2–H_2O interactions illustrate possible mechanisms limiting diffusion in wet MOF structures at $P_{CO_2} < 1$ bar. The method followed to produce such representations is detailed in the Supporting Information text and in Figure S8A–E. We also notice that we have not evidenced strong effects of CO_2 concentrations in water diffusion coefficients (not shown here).

The knowledge of both thermodynamic and equilibrium dynamic parameters (isotherms and self-diffusion coefficients) is a key element to derive a nonequilibrium steady transport equation in highly confined environments such as nanometer MOF pores. In a macroporous medium, fluid transport is well-described by the so-called Darcy equation

$$\mathbf{v} = -\frac{k}{\frac{\eta}{K}}\nabla P \tag{2}$$

which is derived from Navier–Stokes. In eq 2, the flow velocity v scales linearly with the pressure gradient $-\nabla P$ and depends on the ratio of the pore network permeability k and the molecular viscosity η, two intrinsic parameters related to the porous host and the flowing fluid under given thermodynamic conditions, respectively. However, for pores below 50 nm,[60] Darcy's law fails due to slippage, friction, surface tension, nonviscous effects, excess density depending on pore size, and, more generally, to the adsorption dominating transport at the small pore scale.[61−68] Corrections such as the one proposed by Klinkenberg, accounting for slippage, have been included in Darcy's equation.[69] However, such an empirical correction does not capture the phenomenon of molecule adsorption at the pore walls, paramount to describe transport behavior. Such nanoeffects are usually neglected and are certainly difficult to include in continuum fluid approaches due to their discrete nature. Furthermore, nanofluidics is in its infancy and is still poorly understood.[70] To address the question of the transport in nanoporous materials, Bocquet et al.[71] evidenced a linear dependence of v for flowing molecules in pores below 2 nm diameters and thus proposed a nano-Darcy expression, replacing both the permeability and the viscosity in eq 2 by a parameter called "permeance" (K), representing the ability of a fluid to diffuse through a nanoporous slab. This parameter is defined in nanopores as

$$K = \frac{D_s}{\rho k_B T} \tag{3}$$

with ρ the molecular density, k_BT the thermal energy of the system, and k_B the Boltzmann constant. Such an approach has been used in this work to model the transport behavior of CO_2 in UiO-66 for different water loadings. In Figure 6A, we show the host permeance (eq 3) as a function of the CO_2 pressure for different water contents (color plots). K is then used to plot the velocity flow from the nano-Darcy equation as a function of $-\nabla P = \Delta P/L$, with ΔP the differential driving pressure (ranging from 0 to 20 bar) and L the length of the MOF along the flowing direction (with L fixed at 100 nm in these calculations; Figure 6B). As expected from transport equations, we show that the CO_2 velocity (v^{CO_2}) in MOF nanopores scales linearly with $-\nabla P$ for all water loadings accounted (color plots). In Figure 6C, we show v^{CO_2} through UiO-66 as a function of the water loading for different $-\nabla P$ (color plots). v^{CO_2} is found to decrease when the water loading increases, in line with diffusion mechanisms described above, and with K showing a monotonic decrease. Interestingly, when $-\nabla P < 5 \times 10^7$ bar/m ($\Delta P = 5$ bar), a slope change is observed above ~3 wt % and tends to be shifted to larger loading (~10 wt %) for

https://doi.org/10.1021/acs.jpcc.1c09914
J. Phys. Chem. C XXXX, XXX, XXX−XXX

$-\nabla P > 10 \times 10^7$ bar/m. This behavior may be attributed to an increase in driving forces, competing with CO_2 adsorption at water sites, and with the porosity increase of the confined water medium. We finally highlight a surprisingly high ν^{CO_2} of about 1/10 mm/s through the nanoporosity of humid hosts. Such a result is in qualitative agreement with interference microscopy experiments made by Kärger et al.,[72] suggesting that molecular transport in a multiscale porous batch made of MOFs is more limited by the batch porosity (meso- and macropores[60]) than in MOF nanopores.

CONCLUSIONS

In this work, we have highlighted the interplay of CO_2 with H_2O in the Zr-based metal−organic framework UiO-66. Atomistic simulations such as Monte Carlo, performed in the Osmotic ensemble, were used to determine isotherms, accounting for host flexibility effects. This technique is well-suited to reproduce the adsorption behavior of single components when compared to experiments. Using the same methodology, we then show a good agreement with CO_2 adsorption in the MOF for different water loadings, compared to TGA experiments at a CO_2 pressure of 1 bar. Expanding calculations for other CO_2 pressures, we propose a multi-component adsorption diagram, showing a CO_2 enhancement (due to the preadsorbed water), followed by a decrease in the CO_2 uptake compared to dry MOF. The electric field of water acts as a supplemental driving force, in addition to the MOF structure, which explains the excess CO_2 uptake observed. Additionally, water loading can equally lead to a decrease in the CO_2 uptake under some conditions, behaving as an adsorbing competitor in the host porosity. We have thus identified different adsorption regimes in the adsorbent. (i) At a low loading of <1.5 wt %, isolated molecules, or small water nuclei are adsorbed on low-energy sites. (ii) For loadings ranging from ∼1.5 to 3 wt %, nucleation drives cluster formation in octahedral MOF cages. (iii) Between ∼3 and 13 wt %, water clusters weakly bond tetrahedral MOF surfaces. (iv) When loading becomes larger than ∼13 wt %, the water network is found to percolate, forming a sub-nanoporous media in the MOF pores,[73] and then saturate at around 22 wt %. In each case, we found that water tends to lower CO_2 diffusivity due to the attractive nature of CO_2−H_2O interactions, the tortuosity emerging from the sub-nanoporous water network, and the large fraction of the MOF pore volume occupied at large water loading. Finally, from both equilibrium thermodynamic and diffusion data, we used the nano-Darcy equation proposed by Bocquet et al. to gain insight into the CO_2 steady transport behavior for both dry and wet MOF structures. As for equilibrium diffusion, we found that the adsorbed water tends to decrease the CO_2 velocity into the porous network. It is worth noting that we did not observe any CO_2 solubility in confined water clusters under the thermodynamic conditions explored.

The message we would like to address is that while understanding the effects of water on equilibrium CO_2 adsorption is central to many applications, we believe that understanding diffusion and transport behaviors of CO_2 in the presence of H_2O is equally crucial, especially in rapid separation processes. As many applications occur in the presence of humidity, a better fundamental understanding of environmental effects such as (but not limited to) moisture could help in the development of optimal porous materials. As mentioned in the introduction, such materials will be needed for numerous applications, and that could be key to tackle the challenging energy issues that society is facing worldwide.

ASSOCIATED CONTENT

Supporting Information

two and . . The Supporting Information is available free of charge at https://pubs.acs.org/doi/10.1021/acs.jpcc.1c09914.

Additional experimental, methodological, and technical details and figures (PDF)

Lammps input including all parameters for pristine UiO-66 (XYZ)

Lammps input including all parameters for UiO-66 containing a multiphase CO_2−H_2O mixture (XYZ)

AUTHOR INFORMATION

Corresponding Author

⊥**Yann Magnin** − *TotalEnergies@Saclay NanoInnov, 91120 Palaiseau Cedex, France;* orcid.org/0000-0002-4603-632X; Email: yann.magnin@external.totalenergies.com

Authors

Estelle Dirand − *TotalEnergies@Saclay NanoInnov, 91120 Palaiseau Cedex, France*

Alejandro Orsikowsky − *TotalEnergies, OneTech, Sustainability R&D, PERL, 64170 Lacq, France*

Mélanie Plainchault − *TotalEnergies, OneTech, Upstream R&D, CSTJF, 64018 Pau Cedex, France*

Véronique Pugnet − *TotalEnergies, OneTech, Sustainability R&D, CSTJF, 64018 Pau Cedex, France*

Philippe Cordier − *TotalEnergies@Saclay NanoInnov, 91120 Palaiseau Cedex, France*

Philip L. Llewellyn − *TotalEnergies, OneTech, Sustainability R&D, CSTJF, 64018 Pau Cedex, France;* orcid.org/0000-0001-5124-7052

Complete contact information is available at: https://pubs.acs.org/10.1021/acs.jpcc.1c09914

Notes

The authors declare no competing financial interest.

⊥Y.M. is a consultant for TotalEnergies@Saclay NanoInnov, on behalf of TotalEnergies S.E.

ACKNOWLEDGMENTS

This work was supported by TotalEnergies S.E. through OneTech, Sustainability, CCUS R&D project, and CSE and Data Science R&D program. Y.M., E.D., and M.P. also thank TotalEnergies High Performance Computing Center for the CPU time provided on its supercalculator PANGEA II.

REFERENCES

(1) Tapia, J. F. D.; Lee, J.-Y.; Ooi, R. E.; Foo, D. C.; Tan, R. R. A review of optimization and decision-making models for the planning of CO2 capture, utilization and storage (CCUS) systems. *Sustainable Production and Consumption* **2018**, *13*, 1−15.

(2) Lecomte, F.; Broutin, P.; Lebas, E. *CO2 capture: technologies to reduce greenhouse gas emissions*; Editions Technip, 2010.

(3) Gambhir, A.; Tavoni, M. Direct air carbon capture and sequestration: how it works and how it could contribute to climate-change mitigation. *One Earth* **2019**, *1*, 405−409.

(4) Lehtveer, M.; Emanuelsson, A. BECCS and DACCS as negative emission providers in an intermittent electricity system: why levelized cost of carbon may be a misleading measure for policy decisions. *Frontiers in Climate* **2021**, *3*, 15.

(5) Koutsonikolas, D.; Pantoleontos, G.; Mavroudi, M.; Kaldis, S.; Pagana, A.; Kikkinides, E.; Konstantinidis, D. Pilot tests of CO2 capture in brick production industry using gas−liquid contact membranes. *International Journal of Energy and Environmental Engineering* **2016**, *7*, 61−68.
(6) Subramanian Balashankar, V.; Rajendran, A. Process Optimization-Based Screening of Zeolites for Post-Combustion CO2 Capture by Vacuum Swing Adsorption. *ACS Sustainable Chem. Eng.* **2019**, *7*, 17747−17755.
(7) Subraveti, S. G.; Pai, K. N.; Rajagopalan, A. K.; Wilkins, N. S.; Rajendran, A.; Jayaraman, A.; Alptekin, G. Cycle design and optimization of pressure swing adsorption cycles for pre-combustion CO2 capture. *Applied energy* **2019**, *254*, 113624.
(8) Sumida, K.; Rogow, D. L.; Mason, J. A.; McDonald, T. M.; Bloch, E. D.; Herm, Z. R.; Bae, T.-H.; Long, J. R. Carbon dioxide capture in metal−organic frameworks. *Chem. Rev.* **2012**, *112*, 724−781.
(9) Shen, W.; Fan, W. Nitrogen-containing porous carbons: synthesis and application. *Journal of Materials Chemistry A* **2013**, *1*, 999−1013.
(10) Aschenbrenner, O.; McGuire, P.; Alsamaq, S.; Wang, J.; Supasitmongkol, S.; Al-Duri, B.; Styring, P.; Wood, J. Adsorption of carbon dioxide on hydrotalcite-like compounds of different compositions. *Chem. Eng. Res. Des.* **2011**, *89*, 1711−1721.
(11) Belmabkhout, Y.; Serna-Guerrero, R.; Sayari, A. Adsorption of CO2 from dry gases on MCM-41 silica at ambient temperature and high pressure. 1: Pure CO2 adsorption. *Chem. Eng. Sci.* **2009**, *64*, 3721−3728.
(12) Liu, Q.; Pham, T.; Porosoff, M. D.; Lobo, R. F. ZK-5: A CO2-Selective Zeolite with High Working Capacity at Ambient Temperature and Pressure. *ChemSusChem* **2012**, *5*, 2237−2242.
(13) Wang, H.; Jiang, D.; Huang, D.; Zeng, G.; Xu, P.; Lai, C.; Chen, M.; Cheng, M.; Zhang, C.; Wang, Z. Covalent triazine frameworks for carbon dioxide capture. *Journal of Materials Chemistry A* **2019**, *7*, 22848−22870.
(14) Gao, Q.; Bai, L.; Zhang, X.; Wang, P.; Li, P.; Zeng, Y.; Zou, R.; Zhao, Y. Synthesis of Microporous Nitrogen-Rich Covalent-Organic Framework and Its Application in CO2 Capture. *Chin. J. Chem.* **2015**, *33*, 90−94.
(15) Piscopo, C. G.; Loebbecke, S. Strategies to Enhance Carbon Dioxide Capture in Metal-Organic Frameworks. *ChemPlusChem.* **2020**, *85*, 538−547.
(16) Collins, S. P.; Daff, T. D.; Piotrkowski, S. S.; Woo, T. K. Materials design by evolutionary optimization of functional groups in metal-organic frameworks. *Science advances* **2016**, *2*, No. e1600954.
(17) Shekhah, O.; Liu, J.; Fischer, R.; Wöll, C. MOF thin films: existing and future applications. *Chem. Soc. Rev.* **2011**, *40*, 1081−1106.
(18) Li, G.; Xiao, P.; Webley, P.; Zhang, J.; Singh, R.; Marshall, M. Capture of CO2 from high humidity flue gas by vacuum swing adsorption with zeolite 13X. *Adsorption* **2008**, *14*, 415−422.
(19) Merel, J.; Clausse, M.; Meunier, F. Experimental investigation on CO2 post- combustion capture by indirect thermal swing adsorption using 13X and 5A zeolites. *Ind. Eng. Chem. Res.* **2008**, *47*, 209−215.
(20) Boyd, P. G.; Chidambaram, A.; García-Díez, E.; Ireland, C. P.; Daff, T. D.; Bounds, R.; Gładysiak, A.; Schouwink, P.; Moosavi, S. M.; Maroto-Valer, M. M.; et al. Data-driven design of metal−organic frameworks for wet flue gas CO2 capture. *Nature* **2019**, *576*, 253−256.
(21) Benoit, V.; Chanut, N.; Pillai, R. S.; Benzaqui, M.; Beurroies, I.; Devautour-Vinot, S.; Serre, C.; Steunou, N.; Maurin, G.; Llewellyn, P. L. A promising metal−organic framework (MOF), MIL-96 (Al), for CO2 separation under humid conditions. *Journal of Materials Chemistry A* **2018**, *6*, 2081−2090.
(22) Soubeyrand-Lenoir, E.; Vagner, C.; Yoon, J. W.; Bazin, P.; Ragon, F.; Hwang, Y. K.; Serre, C.; Chang, J.-S.; Llewellyn, P. L. How water fosters a remarkable 5-fold increase in low-pressure CO2 uptake within mesoporous MIL-100 (Fe). *J. Am. Chem. Soc.* **2012**, *134*, 10174−10181.
(23) Yazaydın, A. O.; Benin, A. I.; Faheem, S. A.; Jakubczak, P.; Low, J. J.; Willis, R. R.; Snurr, R. Q. Enhanced CO2 adsorption in metal-organic frameworks via occupation of open-metal sites by coordinated water molecules. *Chem. Mater.* **2009**, *21*, 1425−1430.
(24) Kolle, J. M.; Fayaz, M.; Sayari, A. Understanding the Effect of Water on CO2 Adsorption. *Chem. Rev.* **2021**, *121*, 7280.
(25) Frenkel, D.; Smit, B. *Understanding molecular simulation: from algorithms to applications*; Elsevier, 2001; Vol. *1*.
(26) Coudert, F.-X. The osmotic framework adsorbed solution theory: predicting mixture coadsorption in flexible nanoporous materials. *Phys. Chem. Chem. Phys.* **2010**, *12*, 10904−10913.
(27) Peng, D.-Y.; Robinson, D. B. A new two-constant equation of state. *Industrial & Engineering Chemistry Fundamentals* **1976**, *15*, 59−64.
(28) Plimpton, S. Fast parallel algorithms for short-range molecular dynamics. *J. Comput. Phys.* **1995**, *117*, 1−19.
(29) Bambalaza, S. E.; Langmi, H. W.; Mokaya, R.; Musyoka, N. M.; Khotseng, L. E. Experimental Demonstration of Dynamic Temperature-Dependent Behavior of UiO-66 Metal−Organic Framework: Compaction of Hydroxylated and Dehydroxylated Forms of UiO-66 for High-Pressure Hydrogen Storage. *ACS Appl. Mater. Interfaces* **2020**, *12*, 24883−24894.
(30) Wiersum, A. D.; Soubeyrand-Lenoir, E.; Yang, Q.; Moulin, B.; Guillerm, V.; Yahia, M. B.; Bourrelly, S.; Vimont, A.; Miller, S.; Vagner, C.; et al. An evaluation of UiO-66 for gas-based applications. *Chem. Asian J.* **2011**, *6*, 3270−3280.
(31) Rappé, A. K.; Casewit, C. J.; Colwell, K.; Goddard, W. A., III; Skiff, W. M. UFF, a full periodic table force field for molecular mechanics and molecular dynamics simulations. *Journal of the American chemical society* **1992**, *114*, 10024−10035.
(32) Wu, H.; Yildirim, T.; Zhou, W. Exceptional mechanical stability of highly porous zirconium metal-organic framework UiO-66 and its important implications. *journal of physical chemistry letters* **2013**, *4*, 925−930.
(33) Terranova, Z. L.; Paesani, F. The effects of framework dynamics on the behavior of water adsorbed in the [Zn (l-L)(Cl)] and Co-MOF-74 metal−organic frameworks. *Phys. Chem. Chem. Phys.* **2016**, *18*, 8196−8204.
(34) Boyd, P. G.; Moosavi, S. M.; Witman, M.; Smit, B. Force-field prediction of materials properties in metal-organic frameworks. *journal of physical chemistry letters* **2017**, *8*, 357−363.
(35) Campañá, C.; Mussard, B.; Woo, T. K. Electrostatic potential derived atomic charges for periodic systems using a modified error functional. *J. Chem. Theory Comput.* **2009**, *5*, 2866−2878.
(36) Manz, T. A.; Sholl, D. S. Chemically meaningful atomic charges that reproduce the electrostatic potential in periodic and nonperiodic materials. *J. Chem. Theory Comput.* **2010**, *6*, 2455−2468.
(37) Rappe, A. K.; Goddard, W. A., III Charge equilibration for molecular dynamics simulations. *J. Phys. Chem.* **1991**, *95*, 3358−3363.
(38) Potoff, J. J.; Siepmann, J. I. Vapor−liquid equilibria of mixtures containing alkanes, carbon dioxide, and nitrogen. *AIChE journal* **2001**, *47*, 1676−1682.
(39) Horn, H. W.; Swope, W. C.; Pitera, J. W.; Madura, J. D.; Dick, T. J.; Hura, G. L.; Head-Gordon, T. Development of an improved four-site water model for biomolecular simulations: TIP4P-Ew. *J. Chem. Phys.* **2004**, *120*, 9665−9678.
(40) Jajko, G.; Kozyra, P.; Gutiérrez-Sevillano, J. J.; Makowski, W.; Calero, S. Carbon Dioxide Capture Enhanced by Pre-Adsorption of Water and Methanol in UiO-66. *Chemistry (Weinheim an der Bergstrasse, Germany)* **2021**, *27*, 14653−14659.
(41) Hossain, M. I.; Cunningham, J. D.; Becker, T. M.; Grabicka, B. E.; Walton, K. S.; Rabideau, B. D.; Glover, T. G. Impact of MOF defects on the binary adsorption of CO2 and water in UiO-66. *Chem. Eng. Sci.* **2019**, *203*, 346−357.
(42) Ghosh, P.; Colón, Y. J.; Snurr, R. Q. Water adsorption in UiO-66: the importance of defects. *Chem. Commun.* **2014**, *50*, 11329−11331.

https://doi.org/10.1021/acs.jpcc.1c09914
J. Phys. Chem. C XXXX, XXX, XXX−XXX

(43) Cmarik, G. E.; Kim, M.; Cohen, S. M.; Walton, K. S. Tuning the adsorption properties of UiO-66 via ligand functionalization. *Langmuir* **2012**, *28*, 15606−15613.
(44) Yang, Q.; Guillerm, V.; Ragon, F.; Wiersum, A. D.; Llewellyn, P. L.; Zhong, C.; Devic, T.; Serre, C.; Maurin, G. CH 4 storage and CO2 capture in highly porous zirconium oxide based metal−organic frameworks. *Chem. Commun.* **2012**, *48*, 9831−9833.
(45) Canivet, J.; Bonnefoy, J.; Daniel, C.; Legrand, A.; Coasne, B.; Farrusseng, D. Structure−property relationships of water adsorption in metal−organic frameworks. *New J. Chem.* **2014**, *38*, 3102−3111.
(46) Chanut, N.; Bourrelly, S.; Kuchta, B.; Serre, C.; Chang, J.-S.; Wright, P. A.; Llewellyn, P. L. Screening the effect of water vapour on gas adsorption performance: application to CO2 capture from flue gas in metal−organic frameworks. *ChemSusChem* **2017**, *10*, 1543−1553.
(47) Jajko, G.; Gutiérrez-Sevillano, J. J.; Sławek, A.; Szufla, M.; Kozyra, P.; Matoga, D.; Makowski, W.; Calero, S. Water adsorption in ideal and defective UiO-66 structures. *Microporous Mesoporous Mater.* **2022**, *330*, 111555.
(48) Jeremias, F.; Lozan, V.; Henninger, S. K.; Janiak, C. Programming MOFs for water sorption: amino-functionalized MIL-125 and UiO-66 for heat transformation and heat storage applications. *Dalton transactions* **2013**, *42*, 15967−15973.
(49) Sladekova, K.; Campbell, C.; Grant, C.; Fletcher, A. J.; Gomes, J. R.; Jorge, M. The effect of atomic point charges on adsorption isotherms of CO2 and water in metal organic frameworks. *Adsorption* **2020**, *26*, 663−685.
(50) Watanabe, T.; Manz, T. A.; Sholl, D. S. Accurate treatment of electrostatics during molecular adsorption in nanoporous crystals without assigning point charges to framework atoms. *J. Phys. Chem. C* **2011**, *115*, 4824−4836.
(51) Hernandez, A. F.; Impastato, R. K.; Hossain, M. I.; Rabideau, B. D.; Glover, T. G. Water Bridges Substitute for Defects in Amine-Functionalized UiO-66, Boosting CO2 Adsorption. *Langmuir* **2021**, *37*, 10439−10449.
(52) Chen, Q.; Moore, J. D.; Liu, Y.-C.; Roussel, T. J.; Wang, Q.; Wu, T.; Gubbins, K. E. Transition from single-file to Fickian diffusion for binary mixtures in single-walled carbon nanotubes. *J. Chem. Phys.* **2010**, *133*, No. 094501.
(53) Mendonça, B. H.; Ternes, P.; Salcedo, E.; de Oliveira, A. B.; Barbosa, M. C. Water diffusion in carbon nanotubes: Interplay between confinement, surface deformation, and temperature. *J. Chem. Phys.* **2020**, *153*, 244504.
(54) Ghoufi, A.; Szymczyk, A.; Malfreyt, P. Ultrafast diffusion of ionic liquids confined in carbon nanotubes. *Sci. Rep.* **2016**, *6*, 1−9.
(55) Haldoupis, E.; Nair, S.; Sholl, D. S. Efficient calculation of diffusion limitations in metal organic framework materials: a tool for identifying materials for kinetic separations. *J. Am. Chem. Soc.* **2010**, *132*, 7528−7539.
(56) Sharp, C. H.; Bukowski, B. C.; Li, H.; Johnson, E. M.; Ilic, S.; Morris, A. J.; Gersappe, D.; Snurr, R. Q.; Morris, J. R. Nanoconfinement and mass transport in metal−organic frameworks. *Chem. Soc. Rev.* **2021**, *50*, 11530.
(57) Hossain, M. I.; Glover, T. G. Kinetics of water adsorption in UiO-66 MOF. *Ind. Eng. Chem. Res.* **2019**, *58*, 10550−10558.
(58) Skoulidas, A. I.; Sholl, D. S. Self-diffusion and transport diffusion of light gases in metal-organic framework materials assessed using molecular dynamics simulations. *J. Phys. Chem. B* **2005**, *109*, 15760−15768.
(59) Verploegh, R. J.; Nair, S.; Sholl, D. S. Temperature and loading-dependent diffusion of light hydrocarbons in ZIF-8 as predicted through fully flexible molecular simulations. *J. Am. Chem. Soc.* **2015**, *137*, 15760−15771.
(60) Rouquerol, J.; Avnir, D.; Fairbridge, C.; Everett, D.; Haynes, J.; Pernicone, N.; Ramsay, J.; Sing, K.; Unger, K. Recommendations for the characterization of porous solids (Technical Report). *Pure Appl. Chem.* **1994**, *66*, 1739−1758.
(61) Obliger, A.; Pellenq, R.; Ulm, F.-J.; Coasne, B. Free volume theory of hydrocarbon mixture transport in nanoporous materials. *journal of physical chemistry letters* **2016**, *7*, 3712−3717.
(62) June, R. L.; Bell, A. T.; Theodorou, D. N. Molecular dynamics studies of butane and hexane in silicalite. *J. Phys. Chem.* **1992**, *96*, 1051−1060.
(63) Malek, K.; Coppens, M.-O. Knudsen self-and Fickian diffusion in rough nanoporous media. *J. Chem. Phys.* **2003**, *119*, 2801−2811.
(64) Bocquet, L.; Tabeling, P. Physics and technological aspects of nanofluidics. *Lab Chip* **2014**, *14*, 3143−3158.
(65) Won, C. Y.; Aluru, N. Water permeation through a subnanometer boron nitride nanotube. *J. Am. Chem. Soc.* **2007**, *129*, 2748−2749.
(66) Falk, K.; Pellenq, R.; Ulm, F. J.; Coasne, B. Effect of chain length and pore accessibility on alkane adsorption in kerogen. *Energy Fuels* **2015**, *29*, 7889−7896.
(67) Berthonneau, J.; Grauby, O.; Jolivet, I. C.; Gelin, F.; Chanut, N.; Magnin, Y.; Pellenq, R. J.-M.; Ferry, D. Nanoscale Accessible Porosity as a Key Parameter Depicting the Topological Evolution of Organic Porous Networks. *Langmuir* **2021**, *37*, 5464−5474.
(68) Magnin, Y.; Berthonneau, J.; Chanut, N.; Ferry, D.; Grauby, O.; Jorand, R.; Ulm, F. J.; Chaput, E.; Pellenq, R. Hydrocarbon Diffusion in Mesoporous Carbon Materials: Implications for Unconventional Gas Recovery. *ACS Applied Nano Materials* **2020**, *3*, 7604−7610.
(69) Sinha, S.; Braun, E.; Determan, M.; Passey, Q.; Leonardi, S.; Boros, J.; Wood, A.; Zirkle, T.; Kudva, R. In *Steady-state permeability measurements on intact shale samples at reservoir conditions-effect of stress, temperature, pressure, and type of gas*, SPE Middle East oil and gas show and conference; SPE, 2013.
(70) Bocquet, L. Nanofluidics coming of age. *Nature materials* **2020**, *19*, 254−256.
(71) Falk, K.; Coasne, B.; Pellenq, R.; Ulm, F.-J.; Bocquet, L. Subcontinuum mass transport of condensed hydrocarbons in nanoporous media. *Nat. Commun.* **2015**, *6*, 1−7.
(72) Saint Remi, J. C.; Lauerer, A.; Chmelik, C.; Vandendael, I.; Terryn, H.; Baron, G. V.; Denayer, J. F.; Kärger, J. The role of crystal diversity in understanding mass transfer in nanoporous materials. *Nature materials* **2016**, *15*, 401−406.
(73) Hanikel, N.; Pei, X.; Chheda, S.; Lyu, H.; Jeong, W.; Sauer, J.; Gagliardi, L.; Yaghi, O. M. Evolution of water structures in metal-organic frameworks for improved atmospheric water harvesting. *Science* **2021**, *374*, 454−459.

https://doi.org/10.1021/acs.jpcc.1c09914
J. Phys. Chem. C XXXX, XXX, XXX−XXX